October 1996

Radial Dose Distributions in the Delta-Ray Theory of Track Structure

Francis A. Cucinotta
NASA Langley Research Center, Hampton, VA

Robert Katz
University of Nebraska - Lincoln, rkatz2@unl.edu

John W. Wilson
NASA Langley Research Center, Hampton, VA

Rajendra R. Dubey
Old Dominion University

Published in *Two-Center Effects in Ion–Atom Collisions: A Symposium in Honor of M. Eugene Rudd; Lincoln, NE May 1994,* edited by Timothy J. Gay and Anthony F. Starace. AIP Conference Proceedings 362; American Institute of Physics, Woodbury, New York, 1996. Pages 245–265.

Radial Dose Distributions in the Delta-Ray Theory of Track Structure

Francis A. Cucinotta[+], Robert Katz[++], John W. Wilson[+] and Rajendra R. Dubey[*]

[+]*NASA Langley Research Center*
Hampton, VA 23681-0001

[++]*Behlen Laboratory of Physics*
University of Nebraska
Lincoln, NE 68588-0150

[*]*Old Dominion University*
Norfolk, VA 23708

Abstract. The radial dose distribution from delta rays, fundamental to the delta ray theory of track structure, is recalculated. We now include the model of Rudd for the secondary electron spectrum in proton collisions. We include the effects of electron transmission through matter and the angular dependence of secondary electron emission. Empirical formulas for electron range versus electron energy are intercompared in a wide variety of materials in order to extend the track structure theory to arbitrary media. Radial dose calculations for carbon, water, silicon, and gold are discussed. As in the past, effective charge is used to scale to heavier projectiles.

INTRODUCTION

The δ-ray theory of track structure attributes the radiation damage and detection in the passage of heavy ions through matter to the secondary electrons (δ-rays) ejected from the medium by the passing ion (1–5). The track-structure theory has a long history of providing the correct description of a wide variety of phenomenon associated with heavy ion irradiation. Track-structure theory provided the first description of the spatial distribution of energy deposition from ions through the formulation of the radial distribution of dose, as introduced by

Butts and Katz (1) and Kobetich and Katz (2), which led to many experimental measurements of this phenomena (6–10). The response of physical detectors to heavy ions, such as organic scintillators (5), TLD's (5), alanine (11), nuclear emulsion (12), and the Fricke dosimeter (5, 13), have been described using track theory. Many applications in describing biological effects have been made, including the prediction of thindown (5) nearly 20 years prior to the first experimental observation (14) in mammalian cells. More recently, researchers are utilizing track theory in developing improved lithography methods (15) for applications in microelectronics and microtechnology using ion beams.

The radial dose distribution and the geometry of a target site is used in track theory to map gamma-ray response to ion response. The radial dose for intermediate distances from the track is known to fall off as the inverse square of the radial distance to the ion's path, which has led to simplified formulas to be used in many applications (1, 5, 16, 17). It is more difficult to predict the radial dose both near to the ion's path and far from the path due to uncertainties in the electron range versus energy relation, the angular dependence of the secondary electron production cross section, and the effects of δ-ray transport in matter, especially in condensed phase. Many track-structure calculations have used simple, analytic forms for the radial dose from ions which ignore the electron transmission, the angular dependence of electron ejection, and also use simplified electron range-energy relations. In this paper, we consider these factors by following the method of Katz and Kobetich (2, 3, 17) and make new comparisons to recent experimental data for radial dose distributions. An improved model for the secondary electron spectrum in proton collisions with atoms and molecules due to Rudd (19) is used in calculations with the electron spectrum from heavy ions found using scaling by the effective charge of an ion.

RADIAL DOSE FORMALISM

We next review the calculation of the radial dose as a function of radial distance, t, around the path of an ion of atomic number Z, and velocity, β, as introduced by Kobetich and Katz (2–4, 18). In formulating the spatial distribution of energy deposition as charged particles pass through matter, it is assumed that the dominant mode of radial dose deposition is due to electron ejection from the atoms of the target material. The residual energy of an ejected electron (δ-ray) with energy W after penetrating a slab of thickness t is given by the energy to go the residual range $r - t$, as

$$W\left(r,t\right)=\omega\left(r-t\right) \tag{1}$$

where r is taken as the practical range (determined by extrapolating the linear portion of the absorption curve to the abscissa) of an electron liberated with energy ω. The residual energy is then evaluated by Eq. (1) once the range-energy relation in a given target material is known, as discussed below.

The energy dissipated, E, at a depth t by a beam containing one electron per cm^2 is represented in (2) as

$$E = \frac{d}{dt}\left(\eta W\right) \tag{2}$$

where η is the probability of transmission for the electrons. As noted by Kobetich and Katz (4) Eq. (2) neglects several effects. First, it may neglect backscattering, although it may be argued that the energy lost from a layer dt by backscattering is compensated by energy backscattered from later layers. Second, all electrons are represented by an under-scattered class, namely those which penetrate the characteristic distance. Third, the energy deposited by the least-scattered electrons, which penetrate to a thickness $t > r$, is neglected. Such shortcomings could be overcome by direct solution of the electron transport (20) or through the use of Monte-Carlo methods (21). However, the model of Kobetich and Katz has the advantage of simplicity while achieving reasonable accuracy.

The transmission function used will be based on the expressions of Depouy, et al. (22) as modified by Kobetich and Katz (4) and is given by

$$\eta\left(r,t\right) = \exp\left[-\left(qt\ /\ r\right)^{p}\right] \tag{3}$$

with

$$q\ = 0.0059\ Z_T^{0.98} + 1.1 \tag{4}$$

and

$$p\ = 1.8\left(\log_{10} Z_T\right)^{-1} + 0.31 \tag{5}$$

where Z_T is the atomic number of the target material, and r and t are in units of g/cm^2.

In order to estimate the number of free electrons ejected by an ion per unit length of ion path with energies between ω and $\omega + \delta\omega$, the formula given by Bradt and Peters (23) was used by Kobetich and Katz (2)

$$\frac{dn}{d\omega} = \frac{2\pi N Z^{*2} e^4}{mc^2 \beta^2} \frac{1}{\omega^2} \left[1 - \frac{\beta^2 \omega}{\omega_m} + \frac{\pi \beta Z^{*2}}{137} \sqrt{\frac{\omega}{\omega_m}} \left(1 - \frac{\omega}{\omega_m} \right) \right] \tag{6}$$

where e and m are the electron charge and mass, N is the number of free electrons per cm^2 in the target, and ω_m is the classical value for the maximum energy that an ion can transfer to a free electron given by

$$\omega_m = \frac{2mc^2 \beta^2}{1 - \beta^2} \tag{7}$$

In Eq. (6) Z^* is the effective charge number of the ion which is represented by Barkas (24) as

$$Z^* = Z \left[1 - \exp \left(\frac{-125 \beta}{Z^{2/3}} \right) \right] \tag{8}$$

The electron-binding effects are taken into account by Kobetich and Katz (2) following the experimental findings of Rudd et al. (25) who found that ω may be interpreted as the total energy imparted to the ejected electron whose kinetic energy is W, such that ω in Eq. (6) is replaced by

$$\omega = W + I \tag{9}$$

Eq. (6) must be summed for composite materials in which there are N_i electrons per cm^3 having mean excitation energy I_i with values of I_i from Berger and Seltzer (26) and Hutchinson and Pollard (27).

Recently, Rudd (19) has provided a parameterization of the electron spectrum following proton impact based on a binary encounter model modified to agree with Bethe theory at high energies and with the molecular promotion model at low energies. For water, the contributions from five shells are included (19). We also consider this model, scaling to heavy ions using effective charge. In figure 1, we compare the secondary electron spectrum from Eq. (6) to

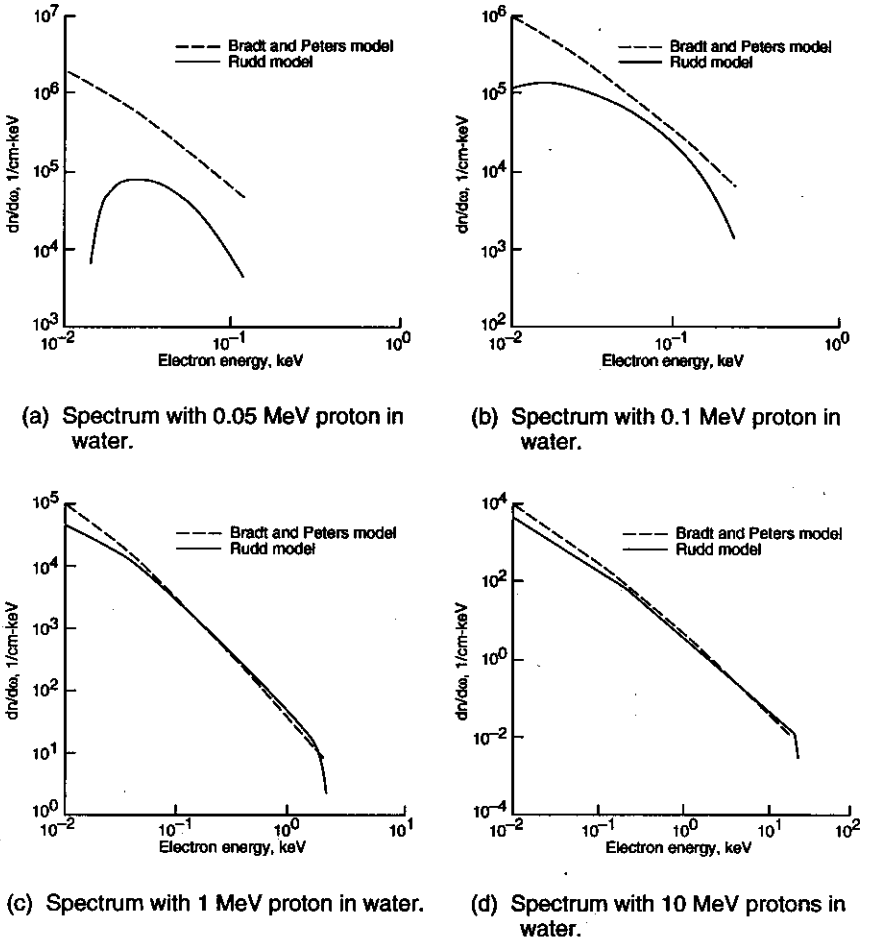

(a) Spectrum with 0.05 MeV proton in water.

(b) Spectrum with 0.1 MeV proton in water.

(c) Spectrum with 1 MeV proton in water.

(d) Spectrum with 10 MeV protons in water.

FIGURE 1. Comparisons of models for secondary electron spectrum from incident protons in water. Shown are a dash-line model of Bradt and Peters (21) and solid-line model of Rudd (18).

the model of Rudd for several proton energies. Large differences between the models occur below proton energies of about 1 MeV and for small electron energies at all proton energies.

Using classical kinematics, electrons of energy ω are ejected at an angle θ to the path of a moving ion given by

$$\cos^2\theta = \frac{\omega}{\omega_m} \tag{10}$$

for the collision between a free electron and the ion. Eq. (10) indicates that close to the ion's path, where distances are substantially less than the range of δ-rays, i.e., $\omega << \omega_m$ and θ is near $\pi/2$, it is sufficient to consider that all δ–rays are normally ejected, and that their energy dissipation in cylindrical shells, whose axis is the ion's path, may be found from knowledge of the energy dissipation of normally incident electrons. Early calculations by Kobetich and Katz (2, 3), showed that assumptions on the angular distribution of δ-rays have little effect on radial dose calculations at intermediate distances where the radial dose falls off as $1/t^2$. If the δ-rays far from an ion's path have an important role on a particular response, then the angular dependence, as well as the dependence of electron range, on the ion's velocity becomes crucial.

If ε is the energy flux carried by δ-rays through a cylindrical surface of radius t whose axis is the ion's path, the energy density E deposited in a cylindrical shell of unit length and mean radius t is given by

$$E = \frac{-1}{2\pi t}\frac{d\varepsilon}{dt} \tag{11}$$

The total energy flux is found by integrating the energy flux carried by a single electron, given by ηW, over the δ-ray distribution and summing over all atoms in the material

$$\varepsilon\left(t\right) = \sum_i \int_{\omega_t}^{\omega_m - I_i} d\omega\, W\left(t,\omega\right)\eta\left(t,\omega\right)\frac{dn_i}{d\omega} \tag{12}$$

The integration limits in Eq. (12) are for the lower limit, ω_t, the energy for an electron to travel a distance t, and upper limit, $\omega_m - I_i$, the maximum kinetic energy that can be given to the electron by the passing ion. Using Eq. (11) and Eq. (12), the energy density distribution may be written as

$$E\left(t\right) = \frac{-1}{2\pi t}\sum_i \int_{\omega_t}^{\omega_m - I_i} d\omega\,\frac{\partial}{\partial t}\left[\eta\left(t,\omega\right)W\left(t,\omega\right)\right]\frac{dn_i}{d\omega} \tag{13}$$

and $E(t)$ is identified as the radial distribution of dose.

In order to consider the angular dependence of the ejected electrons, the energy deposited at a depth t in a slab of material by normally incident electrons is modified by assuming the energy deposited in a cylindrical shell of radius t centered on the ion's path by a delta ray ejected at an angle θ is the same as the energy deposited by an electron normally incident on a slab at depth $t/\sin\theta$ as shown in figure 2. Kobetich and Katz (3) assume that differences between the

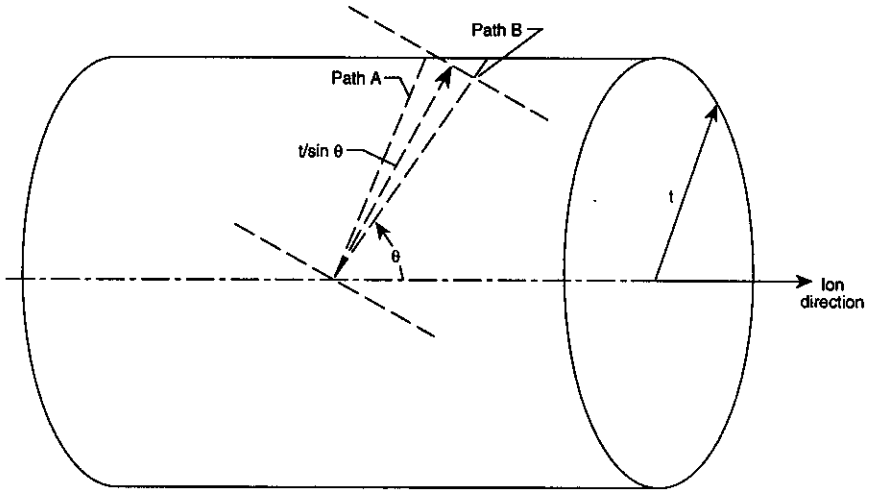

FIGURE 2. The transmission of electrons ejected at an angle to the ion's path through a cylindrical surface of radius *t*.

slab and cylindrical geometries do not greatly affect the energy density distribution, for the differences in the energy density at t caused by those electrons scattered as in path A of figure 2 are compensated by those scattered in path B of figure 2.

The energy density distribution, including an angular distribution of the ejected electrons, is assumed as

$$E\left(t\right)=\frac{-1}{2\pi t}\sum_{i}\int d\Omega\int_{\omega_t\left(\theta\right)}^{\omega_m-I_i}d\omega\,\frac{\partial}{\partial t}\left(\eta\left(t,\omega,\theta\right)W\left(t,\omega,\theta\right)\right)\frac{dn_i}{d\omega d\Omega} \qquad (14)$$

The angular dependence in ω_t, η, and W is through Eq. (10). Experimental measurements for the double differential cross section for electron ejection are sparse and available for only a few ions and mostly modest ion energies (< 10 MeV/amu) (28–31).

A qualitative model for the angular distribution of the secondary electrons is to assume a distribution peaked about the classical ejection value of Eq. (10), such as

$$\frac{dn}{d\omega d\Omega}=\frac{dn}{d\omega}f\left(\theta\right) \qquad (15)$$

with

$$f(\theta) = \frac{N}{\left[\theta - \theta_c(\omega)\right]^2 + \frac{K}{\omega}} \tag{16}$$

with $\theta_c(\omega)$ determined as the root of Eq. (10), N a normalization constant, and K a constant. The constant K may have some dependence on the incident ion's energy and target material, however, is estimated as 0.015 keV from the data of refs. (28–31). Illustrative results of Eqs. (15) and (16) are shown in figure 3, using the model of Rudd (19) for $\frac{dn}{d\omega}$.

RANGE-ENERGY EXPRESSIONS

The electron range-energy relationship is difficult to evaluate theoretically and, because of the complexity of the electron transport problem, empirical expressions based on experimental measurements have been developed by many authors (2, 4, 32–36). Over a limited energy range a power-law of the form, $r = k\omega^{\alpha}$ will be approximately correct and is used by Butts and Katz (1), Zhang, et al. (16), and Kieffer and Stratten (34). The power-law form is useful, since the residual range is easily found by inversion and leads to an analytic

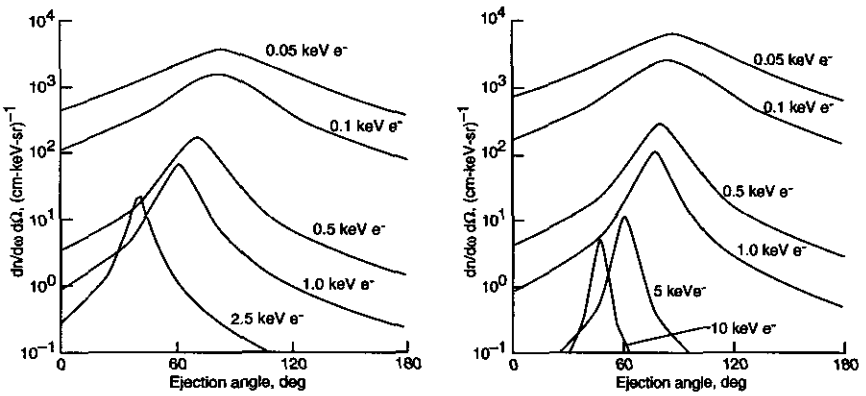

(a) Cross section for 2 MeV protons. (b) Cross section for 10 MeV protons.

FIGURE 3. Model for double differential cross section for electron ejection in water for several proton energies.

form for the radial distribution of dose under the simplifying assumptions of normal ejection and unit electron transmission. A more accurate form as given by Weber (32) and modified by Kobetich and Katz (4) is the ABC formula

$$r = A\omega\left[1 - \frac{B}{1 + C\omega}\right] \tag{17}$$

where

$$A = \left(0.81\, Z_T^{-0.38} + 0.18\right) \times 10^{-3}\ g\ /\ cm^2.\ keV \tag{18}$$

$$B = 0.21\, Z_T^{-0.555} + 0.78 \tag{19}$$

$$C = \left(1.1\, Z_T^{0.29} + 0.21\right) \times 10^{-3}\ keV^{-1} \tag{20}$$

as found by extensive comparison to experimental data for practical range in many materials. Equation (17) is inverted as a quadratic equation to provide $\omega = \omega(r)$.

As a final parameterization, we consider the range formula of Tabata, et al. (33)

$$r = a_1\left[\frac{1}{a_2}\log\left(1 + a_2\tau\right) - a_3\,\tau\left(1 + a_4\,\tau^{a_5}\right)\right] \tag{21}$$

where $t = \omega/m$ and which reduces to Eq. (17) when $a_2\,\tau << 1$ and $a_5 = 1$.

The coefficients in Eq. (21) are

$$\begin{aligned} a_1 &= b_1 A_T\ /\ Z_T{}^{b}2 \\ a_2 &= b_3 Z_T \\ a_3 &= b_4 - b_5 Z_T \\ a_4 &= b_6 - b_7 Z_T \\ a_5 &= b_8\ /\ Z_T{}^{b}6 \end{aligned} \tag{22}$$

with the b_i listed in Table 1. Tabata, et al. (33) provide a parameterization of the inversion of Eq. (21) as

$$\tau = c_1 \left(\exp\left\{ r \left[c_2 + c_3 / \left(1 + c_4 r^{c_5} \right) \right] / c_1 \right\} - 1 \right) \tag{23}$$

with

$$\begin{aligned} c_1 &= d_1 / Z_T \\ c_2 &= d_2 Z_T^{d_3} / A_T \\ c_3 &= d_4 - d_5 Z_T \\ c_4 &= d_6 / Z_T^{d_7} \\ c_5 &= d_8 / Z_T \end{aligned} \tag{24}$$

with the coefficients d_i listed also in Table 1.

A logarithm-polynomial relationship has been used by Iskev, et al. (35) and more recently by Zhang, et al. (36). This however is less useful for the radial dose model since the inversion formula for $\omega = \omega(r)$ is not found easily.

In figure 4, we compare the ABC formula to the expression of Tabata et al. (33) for water where we plot the maximum value of the electron

TABLE 1. Values of the constants b_i and d_i (R_{ex} in g/cm^2)

i	b_i	d_i
1	0.2335 ± 0.0091	(2.98 ± 0.30) x 10^3
2	1.290 ± 0.015	6.14 ± 0.29
3	(1.78 ± 0.36) x 10^{-4}	1.026 ± 0.020
4	0.9891 ± 0.0010	(2.57 ± 0.12) x 10^2
5	(3.01 ± 0.35) x 10^{-4}	0.34 ± 0.19
6	1.468 ± 0.090	(1.47 ± 0.19) x 10^3
7	(1.180 ± 0.097) x 10^{-2}	0.692 ± 0.039
8	1.232 ± 0.067	0.905 ± 0.031
9	0.109 ± 0.017	0.1874 ± 0.0086

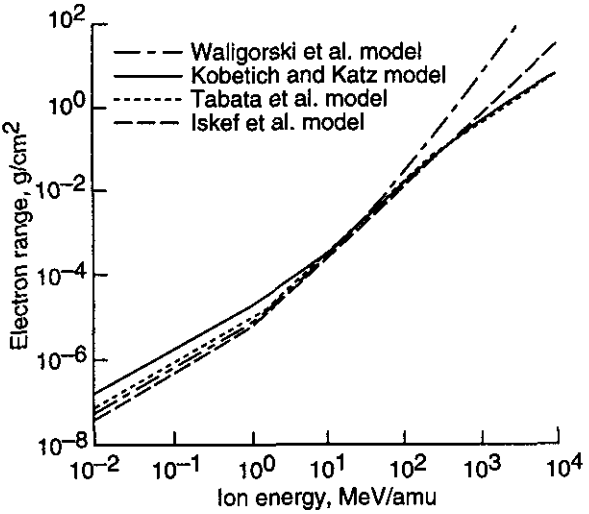

FIGURE 4. Comparison of maximum electron range versus ion energy in water with model of reference (35) shown by dash-dot line, the model of Kobetich and Katz (4) shown by a solid line, model of Tabata et al. (29) shown a by dash line, and model of reference (16) by dotted line.

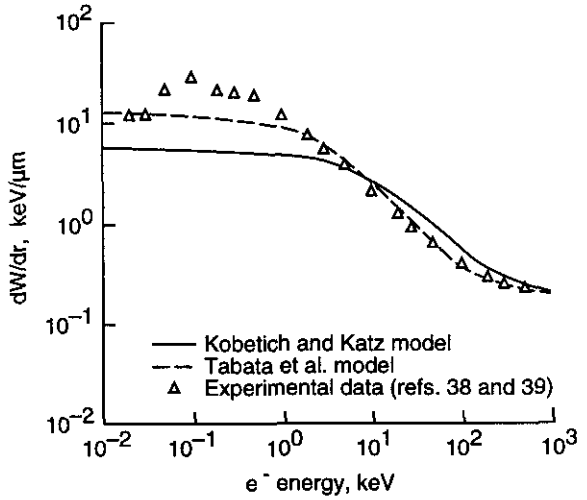

FIGURE 5. Comparison of *dW/dr* in water for model of Kobetich and Katz (4) shown by solid line and of Tabata, et al. (29) shown by dash line to data for electron LET (35, 36).

range versus ion energy using Eq. (7) to relate to the electron energy. The model shown in fig. 4 is for water vapour. We plot versus the ion energy rather than the electron energy to display the maximum width of the ion track for ions of different energies. In the low to intermediate energy range, the formula agrees closely; however, large differences occur below 1 MeV/amu, and above 1000 MeV/amu. These ion energies correspond to electron energies of about 500 keV and 5000 keV, respectively. In figure 4, the formula of Iskev, et al. (35) for water is also shown. In figure 5, we compare dW/dr found from Eq. (16) or Eq. (21) to experimental data (37, 38) for e^- stopping power in water. The model of Tabata et al. (33) agrees well with experiment down to about 1.0 keV, and we will use this model for radial-dose calculations. The differences between the model and experimental data at low electron energy should lead to some uncertainty in radial dose calculations at small impact parameters. Some of the differences that occur between liquid or vapor water have been discussed in ref. (39) and references cited therein and are well known to become important only at low electron energy.

CALCULATIONS OF RADIAL DOSE

In figure 6, we illustrate the effects of electron transmission on calculations of radial dose in water. Calculations are for proton projectiles; however, we note that the radial dose scales approximately as Z^{*2}/β^2 from which results for other ions can be found. The comparison in figure 6 illustrates that the transmission-factor affects the radial dose calculation only very close to and very far from the ion's path with the normalization and expected fall-off as $1/t^2$ unchanged by including the transmission factor.

In figures 7–14, we compare the radial dose calculations to experimental data from refs. (6–9) for several projectiles for ion energies from 0.25 to 377 MeV/amu. In most cases the radial dose measurements are made in tissue equivalent gas. The comparisons to experiments in figs. 7–14 illustrate the fall-off in radial dose of $1/t^2$ in the intermediate distance range. Close to the ion track ($t < 10$ nm) a contribution to the radial dose from molecular excitations contributes as discussed in ref. (39) is expected. It is important to keep the contributions from excitation and ionizations distinct, since it is the secondary electron dose which is assumed to be responsible for most physical effects by heavy ions. At large distances, the inclusion of angular dependence offers a substantial improvement in calculations. The use of the model of Eq. (15) provides an improvement over the classical ejection angle model at the lowest energies (< 2 MeV/amu). At higher energies the model of Eq. (15) appears to underestimate the radial dose at the largest distances. Clearly, more information on the double differential cross section for electron ejection is required.

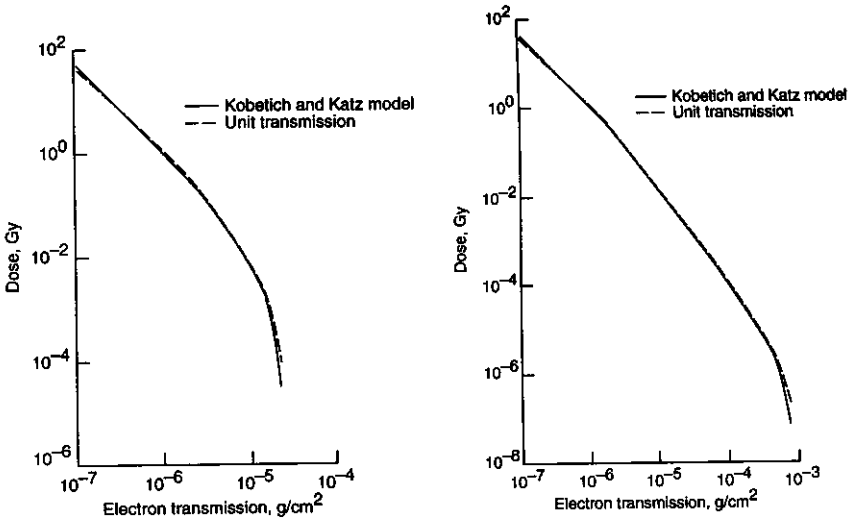

FIGURE 6. Comparison of effects of electron transmission function on calculation of radial dose in water for several proton energies. The solid line is with transmission function of Kobetich and Katz (4), and the dash line assumes unit transmission.

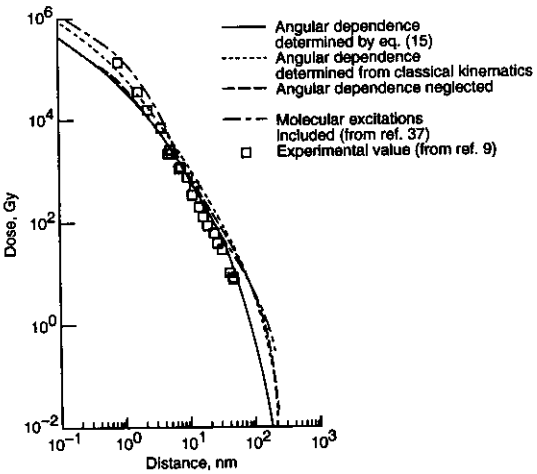

FIGURE 7. Comparison of calculations of radial dose in water for 1 MeV protons to experiment (9). The solid line is with angular dependence of Eq. (15), the dotted line, assuming classical kinematics, the dashed line neglects angular dependence, and the dash-dot line is the result of reference (37), which includes contributions from molecular excitations to radial dose.

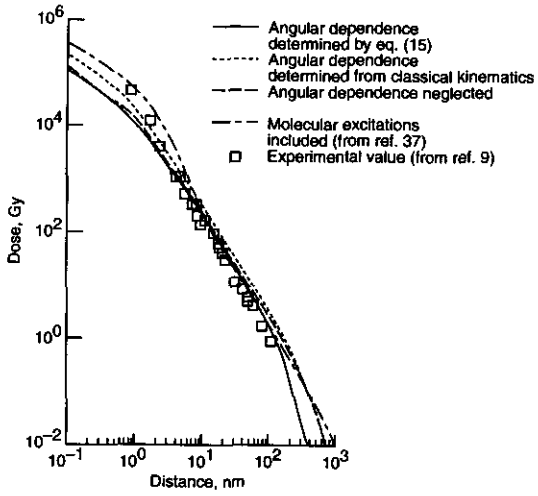

FIGURE 8. Comparison of calculations of radial dose in water for 3 MeV protons to experiment (9). The solid line is with angular dependence of Eq. (15), the dotted line, assuming classical kinematics, the dashed line neglects angular dependence, and the dash-dot line is the result of reference (37), which includes contributions from molecular excitations to radial dose.

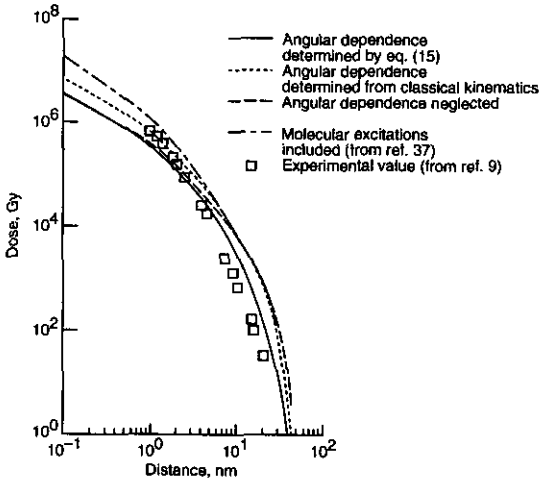

FIGURE 9. Comparison of calculations of radial dose in water for 0.25 MeV/amu ^{4}He ions to experiment (9). The solid line is with angular dependence of Eq. (15), the dotted line assuming classical kinematics, the dashed line neglects angular dependence, and the dash-dot line is the result of reference (37), which includes contributions from molecular excitations to radial dose.

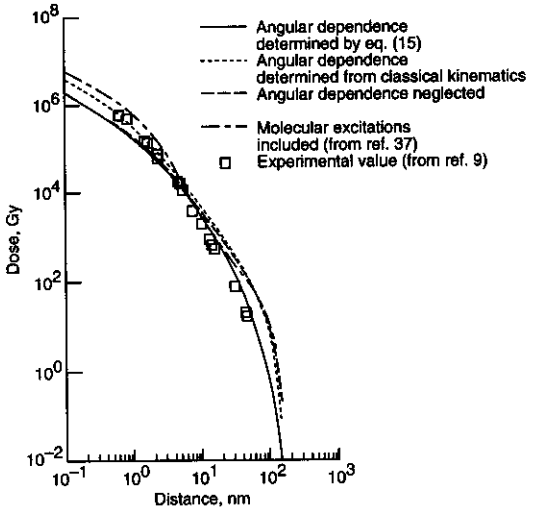

FIGURE 10. Comparison of calculations of radial dose in water for 0.75 MeV/amu ^{4}He ions to experiment (9). The solid line is with angular dependence of Eq. (15), the dotted line assuming classical kinematics, the dashed line neglects angular dependence, and the dash-dot line is the result of reference (33), which includes contributions from molecular excitations to radial dose.

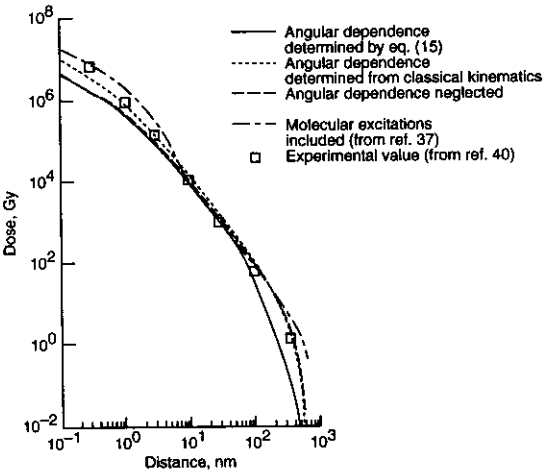

FIGURE 11. Comparison of calculations of radial dose in water for 2.0 MeV/amu ^{12}C to experiment (40). The solid line is with angular dependence of Eq. (15), the dotted line, assuming classical kinematics, the dashed line neglects angular dependence, and the dash-dot line is the result of reference (37), which includes contributions from molecular excitations to radial dose.

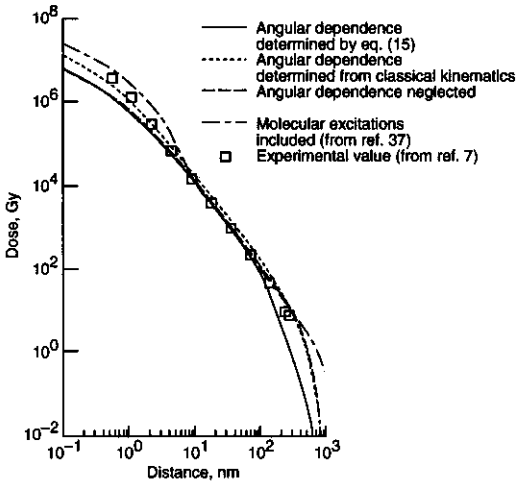

FIGURE 12. Comparison of calculations of radial dose in water for 2.57 MeV/amu ^{16}O to experiment (7). The solid line is with angular dependence of Eq. (15), the dotted line assuming classical kinematics, the dashed line neglects angular dependence, and the dash-dot line is the result of reference (37), which includes contributions from molecular excitations to radial dose.

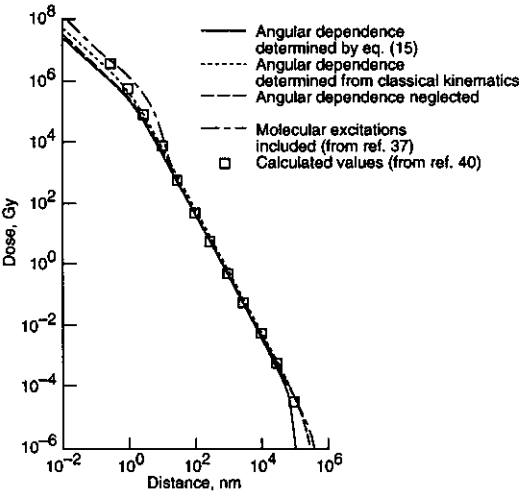

FIGURE 13. Comparison of calculations of radial dose in water for 90 MeV/amu ^{56}Fe with calculations from reference (40). The solid line is with angular dependence of Eq. (15), the dotted line assuming classical kinematics, the dashed line neglects angular dependence, and the dash-dot line is the result of reference (37), which includes contributions from molecular excitations to radial dose.

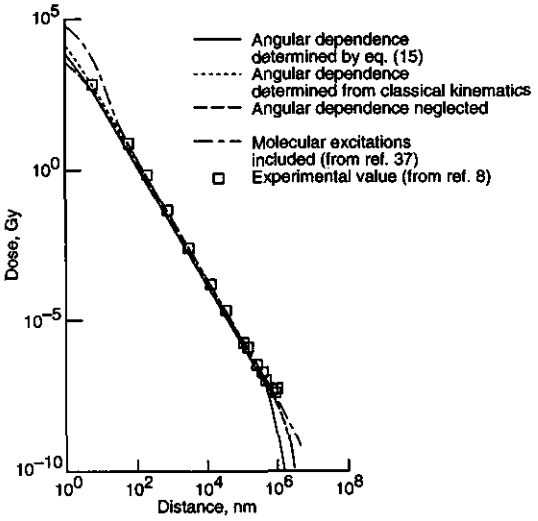

FIGURE 14. Comparison of calculations of radial dose in water for 377 MeV/amu ^{20}Ne to experiment (8). The solid line is with angular dependence of Eq. (15), the dotted line assuming classical kinematics, the dashed line neglects angular dependence, and the dash-dot line is the result of reference (37), which includes contributions from molecular excitations to radial dose.

In figure 15, we illustrate the effects of the radial dose calculations for several velocities in carbon, silicon, and gold. The calculations in figure 15 were made with the secondary electron spectrum of Eq. (6) and assuming classical angular ejection. The model presented in this paper is capable of providing the radial dose for an arbitrary ion in a wide variety of materials, as illustrated by figure 15.

LINEAR ENERGY TRANSFER FROM DELTA RAYS

The contribution to the linear energy transfer (LET) of an ion from delta-rays is evaluated from the radial dose distribution as

$$LET = \int 2\pi t\, E\left(t\right) dt \tag{25}$$

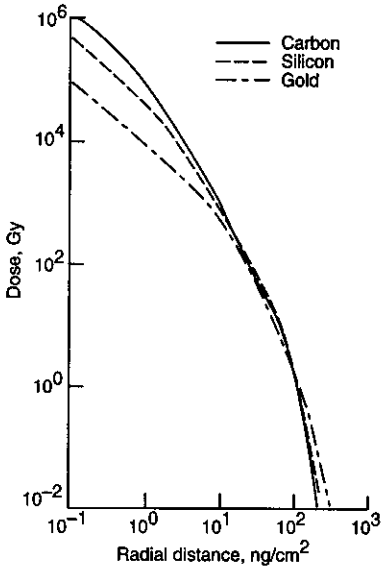

(a) 1 MeV/amu ions.

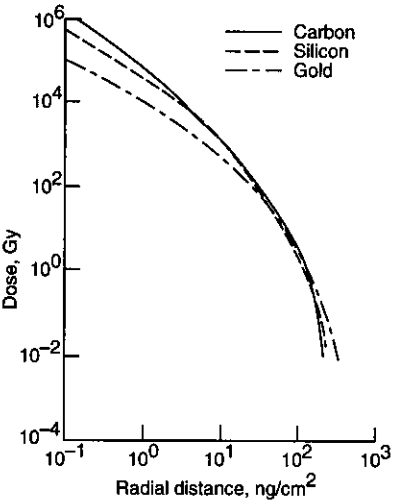

(b) 10 MeV/amu ions.

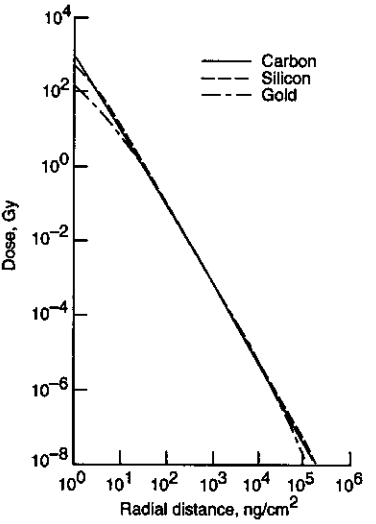

(c) 100 MeV/amu ions.

FIGURE 15. Comparisons of radial dose divided by Z^{*2}/β^2 in carbon, silicon, and gold for several ion energies. Solid line is for carbon, dash line is for silicon, and dash-dot line is for gold.

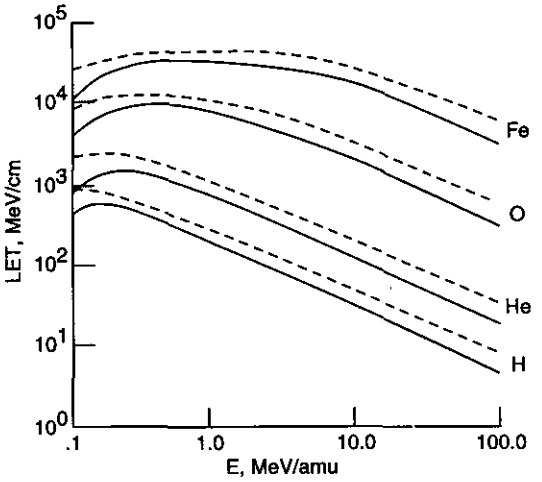

FIGURE 16. Comparisons of the contribution of delta-rays to linear energy transfer (LET) for several ions versus ion energy. Calculated contribution to LET from delta-rays is solid line and fits to measurements of Ziegler (41) is dashed lines.

Calculations of the LET from delta rays are compared to fits to the measurements of Ziegler (41) for several ions in fig. 16. The calculations performed with the present model find about 55–70 percent of the linear energy transfer to be due to the secondary electrons with only a small variation with ion velocity, except below 1 MeV/amu.

CONCLUDING REMARKS

A model for the radial distribution of energy deposited about the path of a heavy ion developed in 1968 by Kobetich and Katz, prior to most experimental measurements of this distribution, is updated with improved physical inputs and compared to experimental data for a variety of ions. Improved models of the electron-range energy and stopping power and the electron-ejection spectra and angular distribution are used in calculations. Excellent agreement with experiment is found. Calculations of the radial dose from heavy ions in water and several materials of interest for spacecraft design and microelectronics were discussed.

REFERENCES

1. Butts, J. J., and Katz, R., *Radiat. Res.* **30**, 855 (1967).
2. Kobetich, E. J., and Katz, R., *Phys. Rev.* **170**, 391 (1968).
3. Kobetich, E. J., and Katz, R., *Phys. Rev.* **170**, 405 (1968).
4. Kobetich, E. J., and Katz, R., *Nucl. Instrum. and Meth.* **71**, 226 (1969).
5. Katz, R., Sharma, S. C., and Homayoonfar, M., in *Topics in Radition Dosimetry. Supplement 1*, New York: Academic Press, 1972.
6. Baum, J. W., Stone, S. L., and Kuehner, A. V., in *Proc. Symp. Microdosim.*, 1968, Ispra, Italy, p. 269.
7. Varma, M. N., Baum, J. W., and Kuehner, A. V., *Radiat Res.* **62**, 1 (1975).
8. Varma, M. N., and Baum, J. W., *Radiat. Res.* **81**, 355 (1980).
9. Wingate, C. L., and Baum, J. W., *Radiat. Res.* **65**, 1 (1976).
10. Metting, N. F., Rossi, H. H., Braby, L. A., Kliauga, P. J., Howard, J., Zaider, M., Schimmerling, W., Wong, M., and Rapkin, M., *Radiat. Res.* **116**, 183 (1988).
11. Hansen, J. W., and Olsen, K. J., *Radiat. Res.* **104**, 15 (1989).
12. Katz, R., and Kobetich, E. J., *Phys. Rev.* **186**, 344 (1969).
13. Katz, R., Sinclair, G, L., and Waligorski, M. P. R., *Nucl. Tracks Radiat. Meas.* **11**, 301 (1986).
14. Kiefer, J., *Int. J. Radiat. Biol.* **48**, 873 (1985).
15. Spohr, R., *Ion Tracks and Microtechnology, Principles and Applications*, Friedr. Vieweg and Son, 1990.
16. Zhang, C., Dunn, D. E., and Katz, R., *Radiat. Protect. Dos.* **13**, 215 (1985).
17. Kobetich, E. J., Ph.D., Thesis, University of Nebraska (1968).
18. Chatterjee, A., and Schaeffer, H. J., *Radiat. Environ. Biophys.* **13**, 215 (1976).
19. Rudd, M. E., *Nucl. Tracks Radiat. Meas.* **16**, 213 (1989).
20. Spencer, L. V., and Fano, U., *Phys. Rev.* **93**, 1172 (1954).
21. Paretzke, H. G., *Proc. Fourth Symposium on Microdosimetry*, 1974, Verbania Pallanza, Italy, p. 141.
22. Depouy, G., Perrier, F., and Arnal, F., *Compt. Rend. Acad. Sci.* (Paris) **258**, 3655 (1964).
23. Bradt, H. L., and Peters, B., *Phys. Rev.* **74**, 1828 (1948).
24. Barkas, W. H., *Nuclear Research Emulsions*. Academic Press Inc., NY, 1963, Vol. 1, 371.
25. Rudd, M. E., Sauter, C. A., and Bailey, C. L., *Phys. Rev.* **151**, 20 (1966).
26. Berger, M. J., and Seltzer S. M., *Natl. Acad. Sci. —Natl. Res. Council, Publ.*, 1964, 1133, 205.
27. Hutchinson, F., and Pollard, E., in *Mechanisms in Radiobiology*, New York: Academic Press, 1961, vol. 1, p. 1.
28. Toburen, L. H., and Wilson, W. E., *J. Chem. Phys.*, **66**, 5202 (1977).
29. Schmidt, S., Kelbch, C., Schmidt-Böcking, H., and Kraft, G., in *Terresterial Space Radiation and its Biological Effects*, New York: Plenum Press, 1988.
30. Rudd, M. E., Toburen, L. H., and Stolterfoht N., *Atomic and Nuclear Data Tables* **18**, 413 (1976).
31. Toburen, L. H., *Phys. Rev.* A **9**, 2505 (1974).
32. Weber, K. H., *Nucl. Inst. Meth.* **25**, 261 (1964).
33. Tabata, T., Ito, R., and Okabe, S., *Nucl. Instrum. Meth.* **103**, 85 (1992).
34. Kieffer, J., and Stratten, H., *Phys. Med. Biol.* **31**, 1201(1986).
35. Iskef, H., Cunningham, J. W., and Watt, D. E., *Phys. Med. Biol.* **28**, 535 (1983).
36. Zhang, C. X., Liu, X. W., Li, M. F., and Luo, D. L., *Radiat. Prot. Dosim.* (1993).
37. Rao, A. R. P., and Fano, U., *Phys. Rev.* **162**, 68 (1967).
38. Cole, A., *Radiat. Res.* **38**, 7 (1969).
39. Waligorski, M. P. R., Hamm, R. N., and Katz, R., *Nucl. Tracks Radiat. Meas.* **11**, 309 (1986).

40. Fain, J., Monnin, M., and Montret, M., *Radiat. Res.* **57**, 379 (1974).
41. Ziegler, J. F., *Nucl. Instrum. and Meth.* **168**, 17 (1980).